Renewable Energy xxx (2016) 1–9

Contents lists available at ScienceDirect

Renewable Energy

journal homepage: www.elsevier.com/locate/renene

Li-ion dynamics and state of charge estimation

Mingheng Li

Department of Chemical and Materials Engineering, California State Polytechnic University, Pomona, CA 91768, United States

ARTICLE INFO

Article history:
Received 30 April 2016
Received in revised form
2 June 2016
Accepted 3 June 2016
Available online xxx

Keywords:
Li-ion
State of Charge
Electrochemical impedance spectroscopy
Extended Kalman filtering
Joint state and parameter estimation

ABSTRACT

This paper focuses on real-time estimation of Li-ion State of Charge (SoC). A first-principles model validated by experimental data from literature is chosen to mimic a real Li-ion cell. Its impedance responses at different SoCs are studied by a simulated electrochemical impedance spectroscopy (EIS). An equivalent circuit model is developed for estimator design in which the parameters (including lumped series resistances R_1, lumped interfacial resistances R_2 and time constant τ) are derived from system identification and compared with the EIS results. The estimator is designed using extended Kalman filtering (EKF) and is implemented in the first-principles model. It is demonstrated by computer simulation that the SoC during charge/discharge cycles can be estimated with a relative error <3%. The accuracy of SoC tracking is improved if it is jointly estimated along with either R_1 or R_2 given that these model parameters vary with SoC as revealed by EIS.

1. Introduction

Rechargeable Li-ion batteries find a wide variety of applications in satellites, electrical vehicles, portable electronics and stationary power storage. In the renewable energy sector, Li-ion batteries may be used in conjunction of photovoltaics [13,28], thermal solar power [22], wind power [27,12], and geothermal applications [14]. It is envisioned that Li-ion batteries will be the promising means of energy storage in off-grid renewable energy given its longer lifespan than other competing technologies (see paper [3] and references therein for detailed discussions).

A Li-ion battery energy storage system may be composed of numerous cells connected in series and/or in parallel configurations to meet specifications of voltage and power. Because of variations in cell manufacturing, a pack consisting of multiple cells is susceptible to State of Charge (SoC) imbalance during operation. A weaker cell becomes depleted faster during discharge while a stronger cell reaches full charge more quickly during charge. To enhance usable battery capacity and to mitigate cell degradation due to over-charge or over-discharge, cell-wise monitoring and control of SoC is desirable in operating high-voltage, high-power Li-ion battery packs.

While techniques exist for direct measurement of the SoC (see review paper [17] and references therein), they have drawbacks limiting their uses in real-time applications. This motivates research and development of model-based state estimation techniques utilizing current and voltage measurements that are readily available during battery operation. Because the Li-ion battery is a nonlinear electrochemical system, nonlinear state estimation techniques such as extended Kalman filtering (EKF) [18,19] and unscented Kalman filtering (UKF) [26,23] could be used. Cell-wise management of a high-power, high-voltage Li-ion pack based on EKF has been successfully demonstrated over a long testing period [24]. The real-time estimator usually employs an equivalent circuit model, in which the SoC is one of the internal states. Calibration of parameters in the equivalent circuit model may be done by minimizing difference in voltages measured experimentally and the model predicted values [9].

The mathematical model plays an important role in EKF-based battery estimator design because it is used in the prediction step of the algorithm to calculate battery state. The equivalent circuit model is a type of lumped parameter model that uses classical electrical elements to capture the main input-output dynamics of Li-ion during charging/discharging cycles [29,10]. It can be easily formulated in the state-space form for model-based estimation and control. To shed an in-depth fundamental understanding of the electrochemical transport phenomena in a Li-ion cell, however, nonlinear first-principles models may be required [5,20]. These models are governed by partial differential equations (PDEs) whose parameters may be tuned to match impedance responses of a real Li-ion cell over a wide spectrum of frequencies [2]. If distributed sensors and actuators are available, model reduction and control

E-mail address: minghengli@cpp.edu.

http://dx.doi.org/10.1016/j.renene.2016.06.009
0960-1481/

design techniques of PDE systems [1] may be applied to the Li-ion cell.

The focus of this paper is on the input-output dynamics of Li-ion. A detailed PDE-based first-principles model from literature that is validated by experimental data [5] is chosen to mimic a real Li-ion cell. An electrochemical impedance spectroscopy (EIS) study is conducted to obtain impedance responses of the cell over a wide spectrum of frequencies. The EIS helps the understanding of cell impedance which significantly affects cycling performance. Furthermore, it reveals that an equivalent circuit model with constant parameters may not be sufficient to capture Li-ion impedance at all SoCs. This motivates joint estimation of SoC with a time-varying battery parameter in real-time estimator design. The estimator is developed utilizing EKF and an equivalent circuit model whose parameters are derived from EIS and battery cycling data. Finally, the joint state and parameter estimator is compared with the state estimator (assuming constant model parameters during battery charge/discharge cycles) using the true SoC value as a baseline.

2. Approach

2.1. First-principles Li-ion model

A lithium-ion cell consists of five regions: a negative electrode current collector, a porous composite negative insertion electrode, a porous separator, a porous composite positive insertion electrode and a positive electrode current collector. In this work, a one-dimensional model is chosen to simulate a cross section of the battery while the edge effect of hight and length is neglected. The model takes into account charge and material balances in the porous electrodes and separator as well as the coupling at the electrode-electrolyte interface. Porous electrode theory is employed so that the medium is treated as a superposition of active material, electrolyte, and filler with known volume fractions [15]. Specifically, the time-dependent PDEs are described as follows:

(i) Charge conservation in homogeneous solid:

$$\nabla\cdot(-\sigma\nabla\varphi_s) = -j^{Li} \tag{1}$$

(ii) Mass conservation in homogeneous solid:

$$\frac{\partial c_s}{\partial t} = \nabla\cdot(D_s\nabla c_s) \tag{2}$$

(iii) Mass conservation in homogeneous electrolyte:

$$\varepsilon_e\frac{\partial c_e}{\partial t} + \nabla\cdot(-D_e\nabla c_e) = \left(\frac{1-t_+^0}{F}\right)j^{Li} \tag{3}$$

(iv) Charge conservation in homogeneous electrolyte:

$$\nabla\cdot(\kappa\nabla\varphi_e + \kappa_D\nabla\ln c_e) = -j^{Li} \tag{4}$$

(v) Lithium-ion movement between solid and electrolyte phases accounting for Butler-Volmer kinetics and double layer capacitance:

$$j^{Li} = a_s i_0\left[\exp\left(\frac{F\eta}{2RT}\right) - \exp\left(-\frac{F\eta}{2RT}\right)\right] + a_s C_{dl}\frac{\partial(\varphi_s-\varphi_e)}{\partial t} \tag{5}$$

In Eqs. (1)–(5), σ is the solid phase conductivity, φ_s is the potential in the solid phase, φ_e is the potential in the electrolyte phase, j^{Li} is the reaction current resulting in production or consumption of Li, t is the time, c is the concentration of lithium ion, D is the diffusion coefficient, F is the Faraday constant, ε is volume fraction, t_+^0 is the transference number, κ is the electrolyte phase conductivity, κ_D is the diffusional conductivity, i_0 is the exchange current density, η is the over-potential, a is the specific area and C_{dl} is the double-layer capacitance. Subscript s represents solid phase and e electrolyte phase, respectively. The Bruggeman relationships are adopted to account for the effect of tortuosity on electrolyte diffusion and ionic conductivity in the above equations. Both cathodic and anodic transfer coefficients are 0.5 to evaluate i_0 using the electrode kinetic equation [5].

Model parameters used in this work are based on a $Li_xC_6|Li_yMn_2O_4$ cell studied by Doyle et al. [5]. The double layer capacitance C_{dl} is assume to be 0.1 F/m^2 [4] and $a_s = 3\varepsilon_s/r_p$, where r_p is the radius of particle in the electrode. The coupled Eqs. (1)–(5) are solved simultaneously using COMSOL Multiphysics, a finite element based numerical solver. The above mathematical model may be enhanced by including side reactions and heat transfer, which will be considered in future work.

2.2. Frequency responses of cell impedance

EIS is a powerful tool to investigate the dynamics of Li-ion cell [2,4,11]. It applies a small excitation voltage or current wave to the electrode and records the resulting response in current or voltage. Excitations at multiple frequencies and various SOCs allow the investigation of several electrochemical transport phenomena occurring at different time scales which facilitates the development of equivalent circuit models for estimator design.

In the EIS simulations, a fully charged cell is first discharged to a specified SoC and then left disconnected for 60 min to allow sufficient relaxation. Subsequently, a small single frequency stimulus current is applied to the positive electrode to observe the response in voltage. A frequency sweep for $f = 10^{-3} - 10^5$ Hz (uniformly distributed in log space) is done to collect 41 sets of data. The whole process is repeated for 11 different SOCs ranging from 0 to 1.

After collecting the current and voltage data, fast Fourier transforms (FFTs) are performed to compute the magnitudes and phase angles of the current and voltage in the transformed domain. For a vector $x = [x_0 x_1 \ldots x_{N-1}]$ with length N, its fast Fourier transform, $X = [X_0 X_1 \ldots X_{N-1}]$, is calculated as follows:

$$X_k = \sum_{n=0}^{N-1} x_n e^{-j(2\pi kn/N)}, k = 0, 1, \ldots, N-1 \tag{6}$$

Given the fact that a single frequency sine wave is used as the stimulus current in each EIS simulation, the voltage output would also be a sine wave with a single frequency assuming quasi-linear response. The magnitude and phase angle of current or voltage are computed as the absolute value and the phase angle of the largest element in the vector of FFT. The complex impedance is then calculated as the transformed voltage divided by the transformed current. The calculation is done for 41 frequencies and 11 SoCs to generate 41 × 11 data points of cell impedance.

2.3. Equivalent circuit model and parameter identification

There are various forms of equivalent circuits available in literature (see, for example [16,9]). It is acknowledged that the equivalent circuit model shown in Fig. 1 provides a reasonable description of battery dynamics during charge/discharge cycles

Please cite this article in press as: M. Li, Li-ion dynamics and state of charge estimation, Renewable Energy (2016), http://dx.doi.org/10.1016/j.renene.2016.06.009

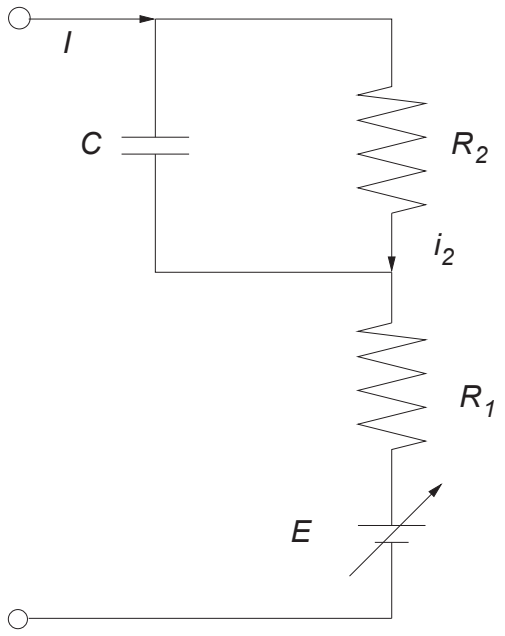

Fig. 1. Equivalent circuit model of a Li-ion cell.

[29]. The circuit involves one parallel resistor-capacitor pair and its mathematical representation is as follows:

$$\begin{aligned} \frac{d}{dt}\begin{bmatrix} i_2 \\ z \end{bmatrix} &= \begin{bmatrix} -1/\tau & 0 \\ 0 & 0 \end{bmatrix}\begin{bmatrix} i_2 \\ z \end{bmatrix} + \begin{bmatrix} 1/\tau \\ \eta_c/C_n \end{bmatrix} I \\ y &= OCV(z) + IR_1 + i_2R_2 \end{aligned} \tag{7}$$

where z is the SoC, $\tau = R_2C$ is the time constant, R_1, and R_2 are resistors and C is the capacitor, i_2 is the current through R_2, I is the overall current (positive for charging and negative for discharging), C_n is the cell capacity, and y is the cell terminal voltage. η_c is the coulombic efficiency (assumed to be 1 in this work). The $OCV(z)$ is the cell open circuit voltage typically obtained by discharging the cell using a small discharge rate [6]. As discussed in literature [29], R_1 represents the lumped series resistances for the solid and liquid phases, R_2 represents the lumped interfacial resistances and C represents the lumped interfacial capacitances.

The discrete-time form of Eq. (7) is given below:

$$\begin{aligned} \begin{bmatrix} i_{2,k+1} \\ z_{k+1} \end{bmatrix} &= \begin{bmatrix} \alpha & 0 \\ 0 & 1 \end{bmatrix}\begin{bmatrix} i_{2,k} \\ z_k \end{bmatrix} + \begin{bmatrix} 1-\alpha \\ \eta_c/C_n \end{bmatrix} I_k \\ y_k &= OCV(z_k) + I_kR_1 + i_{2,k}R_2 \end{aligned} \tag{8}$$

where k is the discrete time index and $\alpha = e^{-\Delta t/\tau}$ (Δt is the time interval).

As pointed out in literature [11] and also the EIS results to be presented later, the parameters α, R_1 and R_2 may not be constant at different SoCs. Moreover, a Li-ion cell ages during operation which leads to slowly increasing R_2 and reduced capacity [24,25,30]. They are usually assumed to be constant to facilitate estimator design while the model-plant mismatch is accounted for in the noise term. The model parameters α, R_1 and R_2 can be determined from EIS data regression (e.g., at a SoC of 50%) or system identification utilizing a set of measured current and voltage data shown below.

Define $\Delta = y - OCV(z)$ as the difference between measured terminal voltage and OCV, a z-transform of Eq. (8) yields:

$$\begin{aligned} zi_2(z) &= \alpha i_2(z) + (1-\alpha)I(z) \\ \Delta(z) &= I(z)R_1 + i_2(z)R_2 \end{aligned} \tag{9}$$

or

$$\frac{\Delta(z)}{I(z)} = \frac{R_1 + (R_2 - \alpha R_1 - \alpha R_2)z^{-1}}{1 - \alpha z^{-1}} \tag{10}$$

whose discrete form in the time domain is:

$$\alpha\Delta_{k-1} + R_1I_k + (R_2 - \alpha R_1 - \alpha R_2)I_{k-1} = \Delta_k \tag{11}$$

For a set of current and voltage data of length N, Eq. (11) may be written as follows:

$$\begin{bmatrix} \Delta_1 & I_2 & I_1 \\ \Delta_2 & I_3 & I_2 \\ \vdots & & \\ \Delta_{N-1} & I_N & I_{N-1} \end{bmatrix}\begin{bmatrix} \alpha \\ R_1 \\ R_2 - \alpha R_1 - \alpha R_2 \end{bmatrix} = \begin{bmatrix} \Delta_2 \\ \Delta_3 \\ \vdots \\ \Delta_N \end{bmatrix} \tag{12}$$

The above equation is in the standard matrix form of $Ax = b$ whose optimal solution is $x = (A^TA)^{-1}A^Tb$. Based on the solution α, R_1 and R_2 are easily determined. It is worth pointing that the same approach may be applied to determine model parameters in more complicated equivalent circuit models involving multiple parallel resistor-capacitor pairs in series.

2.4. SoC estimator design

The SoC estimator may be designed with/without the estimation of Li-ion cell parameters. In either case, observability issues should be carefully considered. A necessary condition for bounded estimation error when applying EKF to a nonlinear system is that all states of the system are observable [21]. It is shown that the rank of the observability matrix should be equal to the total number of states and parameters. For the Li-ion system which has only one measured output, it means that the observability matrix of the augmented system should be non-singular. It has been verified that at most one Li-ion cell parameter (either R_1 or R_2 but not both) may be jointly estimated along with the states ($i_{2,k}$ and z_k) in the estimator design if the equivalent circuit model of Eq. (8) is used. Without showing the detailed math, a simple explanation is given as follows. If a constant I is applied in Eq. (8) for a sufficient amount of time, i_2 will approach I, and an independent filtering of R_1 and R_2 becomes infeasible. Therefore, at most one resistor in Eq. (8) may be treated as a time-varying parameter during battery charge/discharge cycles. For Kalman filtering of linear systems with time-varying parameters, it is proved that the parameter tracking errors are small when the parameter variation and process noise are small [7].

In the following paragraphs, details of joint estimation of SoC and R_2 (assuming fixed R_1) using EKF will be provided. The joint estimation of SoC and R_1 (assuming fixed R_2) or state estimation of SoC (assuming fixed R_1 and R_2) may be formulated in a similar way.

To jointly estimate SoC and R_2, the following discrete state-space form of the augmented system is used:

$$\begin{aligned} x_{k+1} &= \mathbb{A}_kx_k + \mathbb{B}_kI_k + [\omega_{1,k}\ \omega_{2,k}\ \xi_k]^T \\ y_k &= OCV(z_k) + i_{2,k}R_{2,k} + I_kR_1 + \nu_k \end{aligned} \tag{13}$$

where $x_k = [i_{2,k}\ z_k\ R_{2,k}]^T$, $\mathbb{A}_k = \mathrm{diag}([\alpha,1,1])$, $\mathbb{B}_k = [1-\alpha\ \eta_c/C_n\ 0]^T$, $\omega_{1,k}$ and $\omega_{2,k}$ are the unmeasured the process noises, and ν_k is the measurement noise. Here $\mathrm{diag}(a_1,\ldots,a_n)$ stands for a diagonal matrix whose diagonal entries starting from the upper left corner are a_1, …, and a_n.

Please cite this article in press as: M. Li, Li-ion dynamics and state of charge estimation, Renewable Energy (2016), http://dx.doi.org/10.1016/j.renene.2016.06.009

The state and input matrices in Eq. (13) are already in a linear form. The linearized output matrix is $\mathbb{C}_k = \left[R_{2,k-1} \ \frac{dOCV(z)}{dz}|_{k-1} \ i_{2,k-1}\right]$ based on Taylor expansion of y_k around the battery state at time index $k-1$. Let $\mathbb{Q}_k$ be the covariance matrix for the process noise of the augmented system, $[\omega_{1,k} \ \omega_{2,k} \ \xi_k]^T$ and R_k be the covariance of the measurement noise ν_k, the Kalman filtering algorithm can be applied as follows:

(i) State estimate time update: $\widehat{x}_k^- = \mathbb{A}_{k-1}\widehat{x}_{k-1} + \mathbb{B}_{k-1}I_{k-1}$
(ii) Error covariance time update: $\mathbb{P}_k^- = \mathbb{A}_{k-1}\mathbb{P}_{k-1}\mathbb{A}_{k-1}^T + \mathbb{Q}_{k-1}$
(iii) Kalman gain matrix: $\mathbb{L}_k = \mathbb{P}_k^-\mathbb{C}_k^T[\mathbb{C}_k\mathbb{P}_k^-\mathbb{C}_k^T + R_k]^{-1}$
(iv) State estimate measurement update: $\widehat{x}_k = \widehat{x}_k^- + \mathbb{L}_k(y_k - OCV(\widehat{z}_k^-) - \widehat{i}_{2,k}^- R_{2,k}^- - I_k R_1)$
(v) Error covariance measurement update: $\mathbb{P}_k = (\mathbb{I} - \mathbb{L}_K\mathbb{C}_k)\mathbb{P}_k^-$

In the above steps, $\mathbb{L}$ is the Kalman gain matrix and $\mathbb{I}$ is the identity matrix. With initial values of $i_{2,0}$, z_0, $R_{2,0}$ and $\mathbb{P}_0$, repeating (i)–(v) using measured current input and voltage output will solve SoC and R_2 at all time steps.

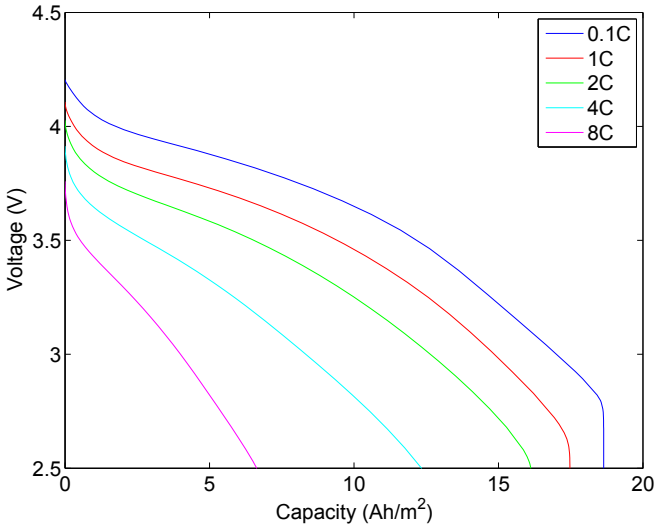

Fig. 2. Relationship between battery capacity and discharge rate.

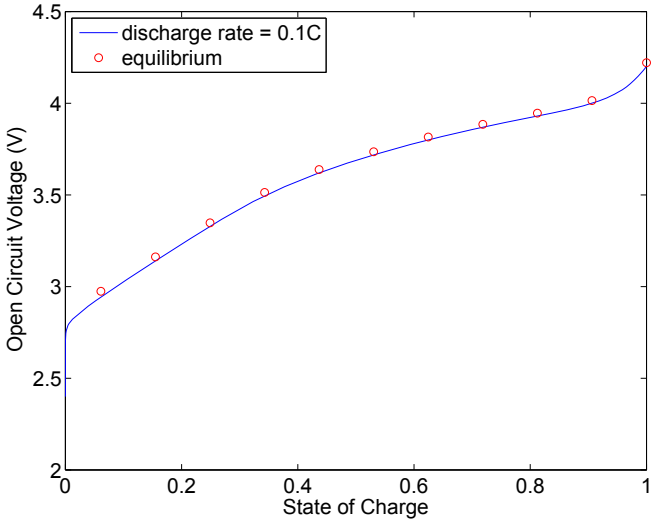

Fig. 3. Open circuit voltage curve.

The $OCV(z)$ in this work is determined along with the EIS simulation, and there are 11 discrete data points in total. While polynomial has been used to fit the curve in literature, it is believed

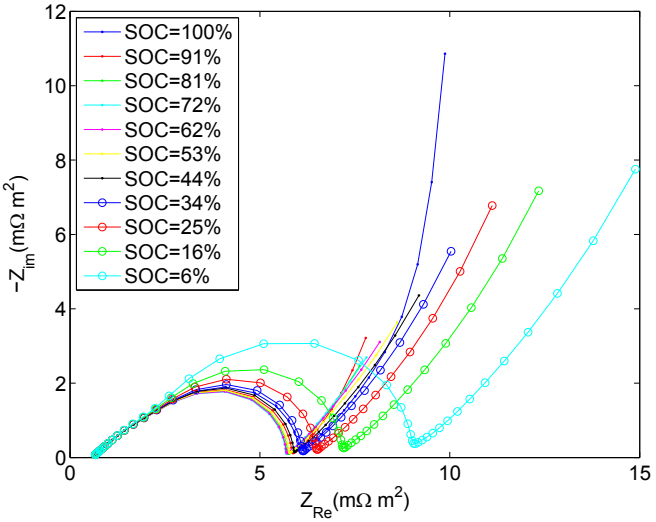

Fig. 4. Nyquist plot of cell impedance.

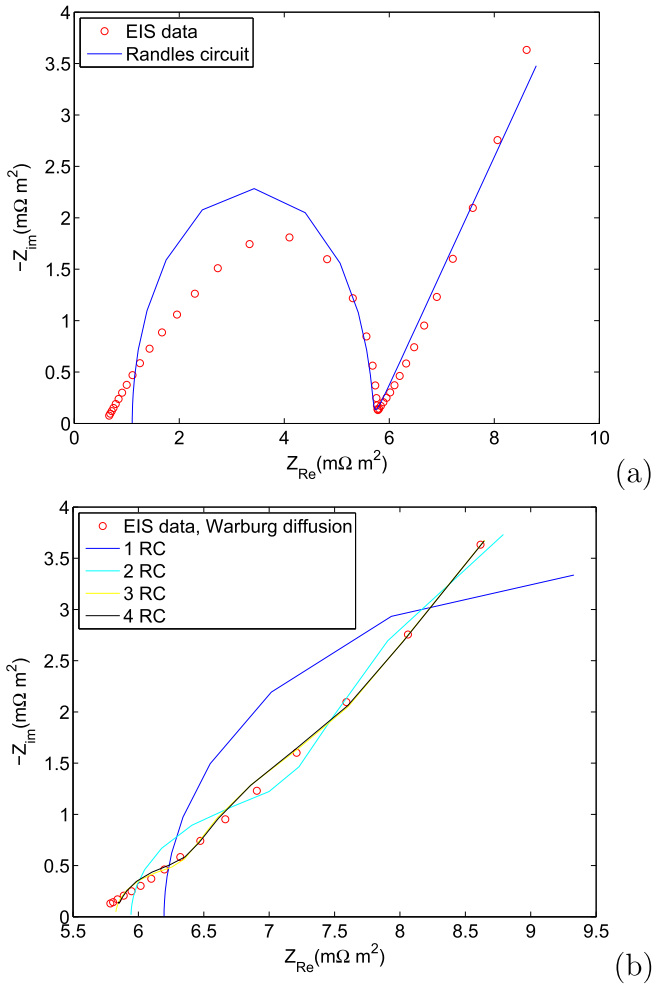

Fig. 5. Fitting of EIS data at 53% SoC using (a) the Randles circuit model and (b) one or multiple parallel resistor-capacitor pairs connected in series.

Please cite this article in press as: M. Li, Li-ion dynamics and state of charge estimation, Renewable Energy (2016), http://dx.doi.org/10.1016/j.renene.2016.06.009

that cubic spline interpolation provides better results of $OCV(z)$ [8]:

$$OCV(z) = a_i + b_i z + c_i z^2 + d_i z^3,\ z_i < z \le z_{i+1},\ i = 1, 2, \ldots, 10 \tag{14}$$

where a_i, b_i, c_i and d_i are parameters for the i^{th} interval between z_i and z_{i+1}. 4×10 parameters are to be determined based on the $OCV(z)$ data. The derivative of OCV with respect to SoC may be calculated as below:

$$\frac{d}{dz}OCV(z) = b_i + 2c_i z + 3d_i z^2,\ z_i < z \le z_{i+1},\ i = 1, 2, \ldots, 10 \tag{15}$$

To jointly estimate R_1 and SoC assuming a constant R_2, the matrix $\mathbb{C}_k$ in the above equations should be replaced by $\left[R_{2,k-1}\ \frac{dOCV(z)}{dz}\big|_{k-1}\ I_{k-1}\right]$. For state estimation using fixed R_1 and R_2 derived from Eq. (12), the dimension of the system is 2 instead of 3. Therefore, the matrices $\mathbb{A}$, $\mathbb{B}$, $\mathbb{C}$, $\mathbb{Q}$, $\mathbb{P}$ and $\mathbb{I}$ should be truncated accordingly, i.e. the last column and/or row should be removed.

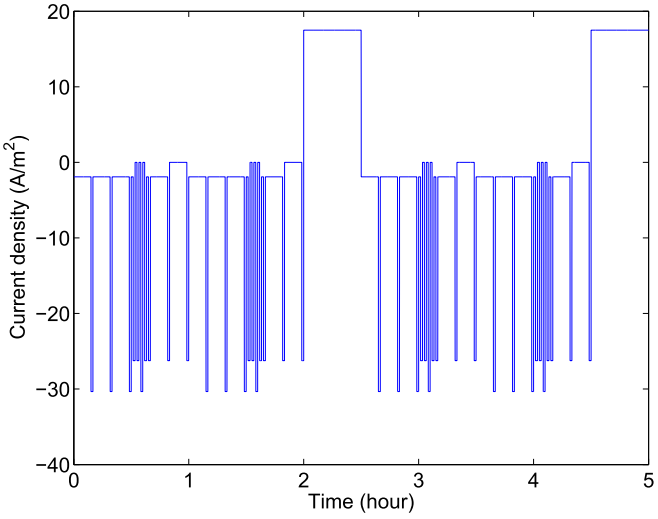

Fig. 6. Profiles of current density input.

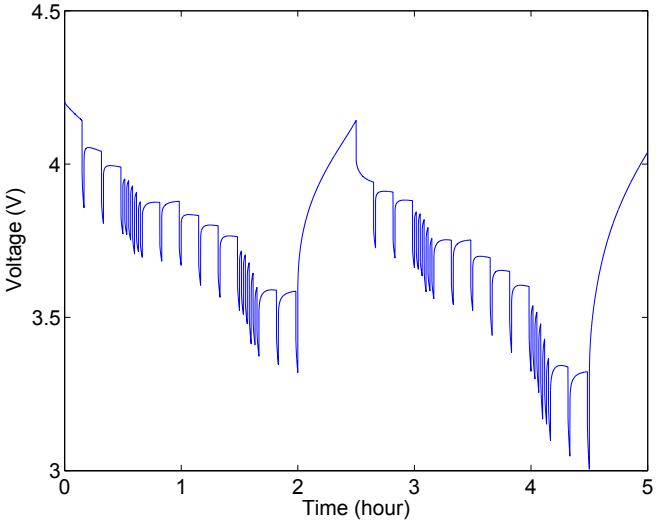

Fig. 7. Profiles of terminal voltage output.

3. Results and discussion

The Li-ion cell capacity is determined by solving Eqs. (1)–(5) in which a fully charged cell is discharged at five constant rates (0.1C, 1C, 2C, 4C and 8C; 1C = 17.5 A/m^2 [5], or the current density that

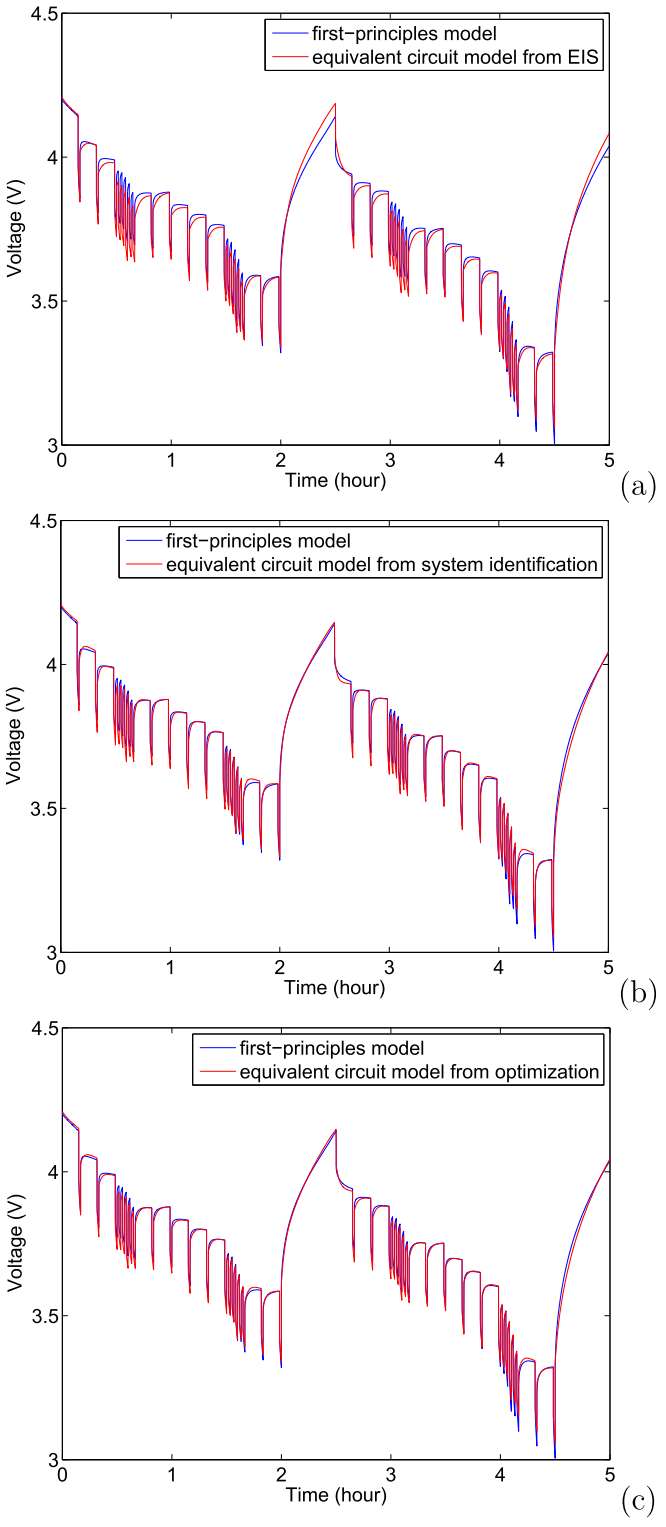

Fig. 8. Comparison between terminal voltage from first-principles model with the one from equivalent circuit model whose parameters are derived from (a) EIS data at 53% SoC, (b) system identification and (c) optimization.

Please cite this article in press as: M. Li, Li-ion dynamics and state of charge estimation, Renewable Energy (2016), http://dx.doi.org/10.1016/j.renene.2016.06.009

will discharge the battery in 1 h) until the terminal voltage drops below 2.5 V. The results are shown in Fig. 2. Clearly, the effective cell capacity reduces when a higher discharge rate is used. For example, it is 18.64 Ah/m^2 at 0.1C discharge rate, 17.5 Ah/m^2 at 1C, and only 6.5 Ah/m^2 at 8C. This is mainly because of cell internal impedance, causing the terminal voltage during discharge smaller than the OCV.

To obtain the OCV curve in this work, the 0.1C discharge curve in Fig. 2 is normalized by its maximum, or 18.64 Ah/m^2, which corresponds to 100% SoC. The result is shown by the curve in Fig. 3. However, if sufficient relaxation (1 h in this work) is allowed after the cell reaches a specific SoC during the discharging process, its voltage increases slightly, as shown by the circle symbols in the same figure. This is because the 0.1C discharge rate, even though small, is not zero. These 11 data points are therefore chosen for cubic spline interpolation in Eq. (14).

The Nyquist plots derived from the EIS simulations are shown in Fig. 4. At each SoC, the curve is similar to the impedance response of a Randles circuit:

$$Z(w) = R_s + \frac{1}{\frac{1}{(jw)C_{dl}} + \frac{1}{R_{ct}+\frac{1}{Q(jw)^n}}} \tag{16}$$

where R_s is the electrolyte resistance, R_{ct} is the charge transfer resistance, C_{dl} is the double layer capacitance, and the Warburg diffusion is simulated as a constant phase element (CPE) whose impedance is $Z(w) = 1/Q(jw)^n$. For example, when SoC = 53%, data regression of the impedance response yields $R_s = 0.0011\ \Omega\ m^2$, $R_{ct} = 0.0045\ \Omega\ m^2$, $C_{dl} = 0.3385\ F/m^2$, $Q = 3647(\Omega\ m^2)^{-1}\ s^{-0.53}$ and $n = 0.53$. A comparison between the EIS data and the Randles circuit is shown in Fig. 5(a). The time constant in the kinetic arc is estimated to be 2 ms ($=R_{ct}C_{dl}$), which is much smaller than the characteristic time scales of battery cycling dynamics in most applications. By ignoring the double layer capacitance term from Eq. (16) and approximating the CPE with multiple parallel resistor-capacitor (RC) pairs connected in series at frequencies at 1 Hz and above, the cell impedance can be realized in the time domain, as shown in Fig. 5(b). If only one RC pair is used, the circuit collapses to the shown in Fig. 1, which is of interest in this work. While an equivalent circuit model employing more parallel RC pairs in series fits the EIS data at a single SoC (i.e. 53%) better, it does not necessarily represent the cell impedances at other SoCs because the impedance response curves at different SoCs shown in Fig. 4 do not overlap. In this sense, an equivalent circuit model with constant parameters may not be sufficient to describe a Li-ion cell at all SoCs, regardless of the number of RC pairs included in the model.

Fig. 6 shows the current density profile used in cycling test in this work. The Li-ion cell goes through discharge at various C-rates and charge at a constant 1C rate. The corresponding terminal voltage calculated from the first principles model is shown in Fig. 7. The time interval in both data sets is 1 s. A comparison of terminal voltage predicted by the equivalent circuit model using parameters from EIS data at 53% SoC and the measured voltage (or the voltage from the first-principles model) is given in Fig. 8(a). It is found that using more RC pairs in the model does not yield superior results

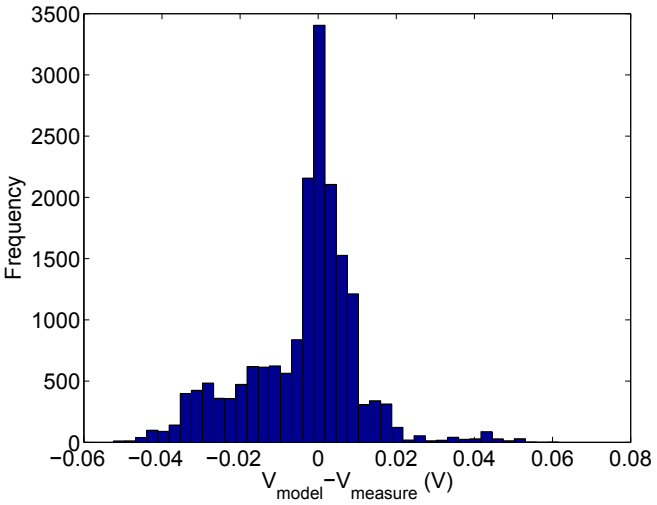

Fig. 9. Distribution of model-plant mismatch.

(not shown here), despite a better fit of EIS data at single SoC of 53%. Two other methods are also used to determine the parameters in the equivalent circuit model involving only one RC circuit represented by Fig. 1. Based on Eq. (12), the parameters are determined to be $R_1 = 0.0058\ \Omega\ m^2$, $R_2 = 0.0048\ \Omega\ m^2$ and $\alpha = 0.9862$. The corresponding time constant $\tau = -\Delta t/\ln(\alpha) = 72$ s. The model predicted voltage profile is shown in Fig. 8(b). If these parameters are used as initial guesses in an optimization to minimize modeling error, $R_1 = 0.0063\ \Omega\ m^2$, $R_2 = 0.0043\ \Omega\ m^2$ and $\alpha = 0.9910$ (or $\tau = 111$ s). The model predicted voltage profile is shown in Fig. 8(c). A summary of mean and standard deviation of modeling errors is provided in Table 1. It appears that the equivalent circuit model using one RC pair with all three sets of parameters provides reasonable results of terminal voltage. The model-plant mismatch may be explained by model simplification as well as constant R_1, R_2 and τ used for all SoCs. When the EKF is used, the modeling error may be included in the noise term. In the following paragraphs, the model parameters are based on the results from Eq. (12), whose modeling error is shown in Fig. 9. A comparison of EKF results using different model parameters derived from all three approaches will be presented later.

In EKF of battery SoC, the final estimation is based on an optimal combination of model predictions and terminal voltage measurements. The covariances of the process noise and the measurement noise gauge the fidelity of the model and the measurement, and therefore, are important in order for the algorithm to perform accurately. Given the fact that the model-plant mismatch is much greater than the noise of typical data acquisition units (on the order of 0.1 mV), the covariance of the measurement noise R_k is chosen to be 0.0143^2 or 2×10^{-4}. Moreover, the process noises are assumed to be mutually independent and $\mathbb{Q}_k$ is chosen to be diag(10^{-4},10^{-10},10^{-8}) in joint estimation and diag(10^{-4},10^{-10}) in state estimation. These numbers are selected based on the magnitude of i_2 and z. $\mathbb{P}_0$ is chosen to be diag(10^{-5},10^{-5},10^{-6}) for joint estimations

Table 1
Mean and standard deviation of error in the equivalent circuit model using parameters from different approaches. R is in $\Omega\ m^2$, τ is in second, and mean/standard deviation of modeling error of voltage is in V.

Approach	R_1	R_2	τ	Mean of error	Std. dev. of error
EIS data at 53% SoC (Fig. 5)	0.0062	0.0067	169	−0.0070	0.0236
System identification (Eq. (12))	0.0058	0.0048	72	−0.0035	0.0143
Optimization	0.0063	0.0043	111	−0.0038	0.0133

Please cite this article in press as: M. Li, Li-ion dynamics and state of charge estimation, Renewable Energy (2016), http://dx.doi.org/10.1016/j.renene.2016.06.009

and diag(10^{-5},10^{-5}) for state estimation. Three initial guesses of SoC, 0.5, 0.6 and 0.7, are chosen to verify whether the EKF algorithms can converge to the same solution.

Three EKF estimators are tested using current input and voltage output data from the first principles model: (1) joint estimation of SoC and R_2 (R_1 is fixed to be 0.00579 Ωm^2), (2) joint estimation of SoC and R_1 (R_2 is fixed to be 0.00481 Ωm^2) and (3) state estimation

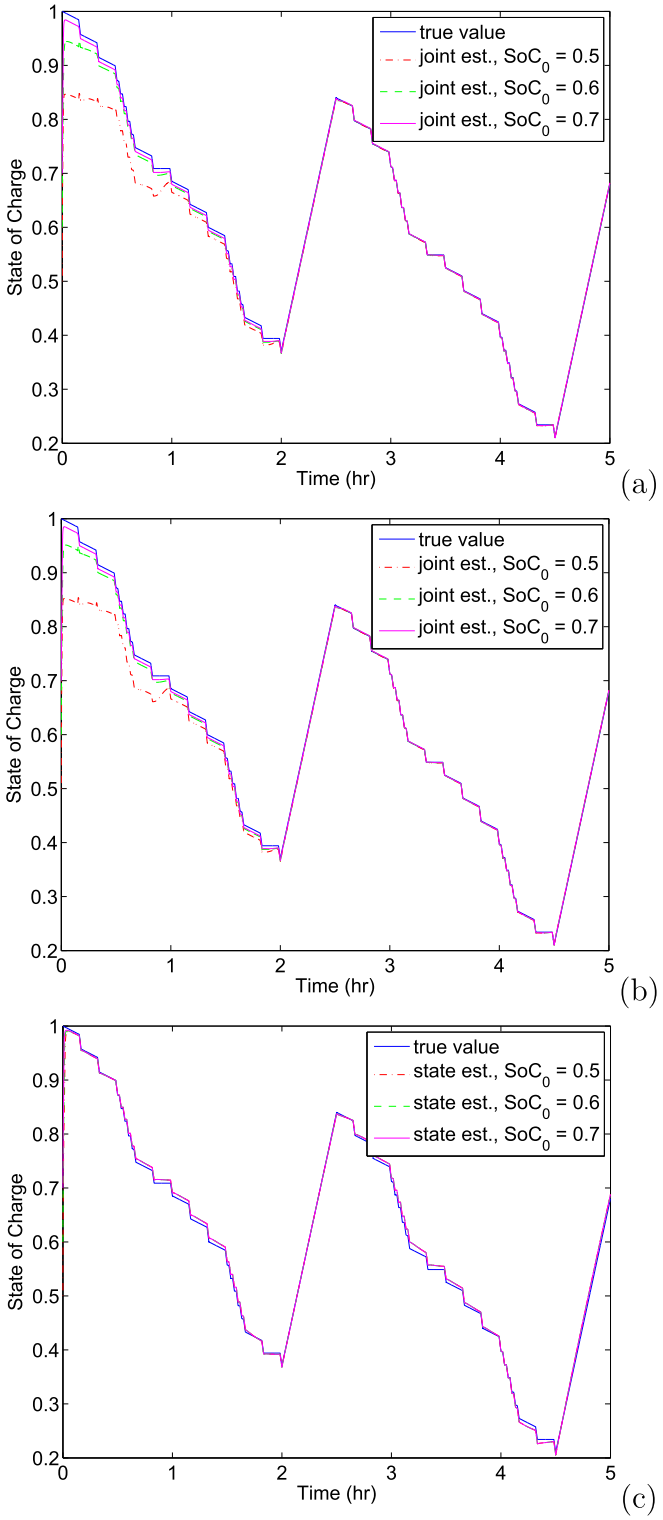

Fig. 10. Comparison of SoC estimated by three algorithms and its true value from coulomb counting: (a) joint estimation of SoC and R_2 (R_1 is fixed at 0.0058 Ω m^2), (b) joint estimation of SoC and R_1 (R_2 is fixed at 0.0048 Ω m^2), and (c) state estimation of SoC (R_1 is fixed at 0.0058 Ω m^2 and R_2 is fixed at 0.0048 Ω m^2).

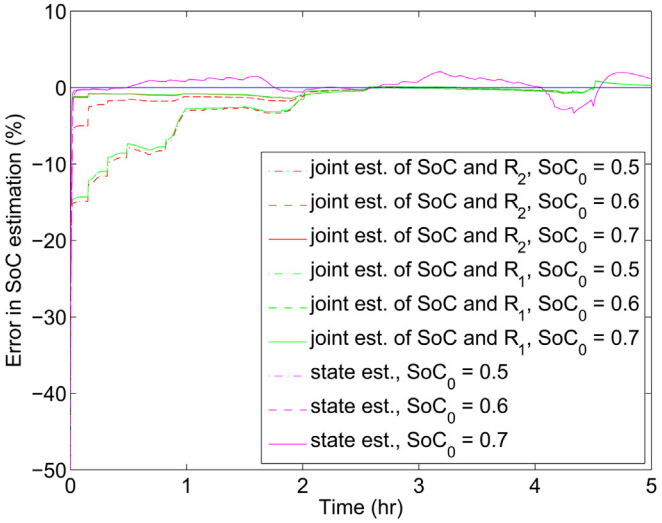

Fig. 11. Estimation error of all algorithms with different initial values of SoC.

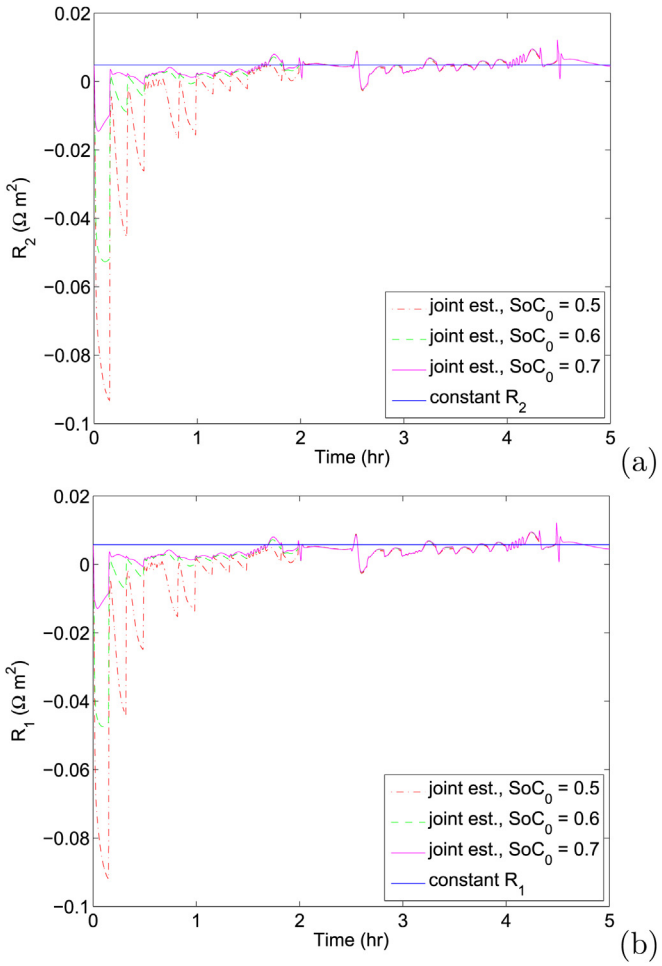

Fig. 12. Estimation of battery parameter in joint state/parameter estimation (a) joint estimation of R_2 and SoC (R_1 is fixed at 0.0058 Ω m^2) and (b) joint estimation of R_1 and SoC (R_2 is fixed at 0.0048 Ω m^2).

Please cite this article in press as: M. Li, Li-ion dynamics and state of charge estimation, Renewable Energy (2016), http://dx.doi.org/10.1016/j.renene.2016.06.009

of SoC (R_1 is fixed to be 0.00579 Ωm^2 and R_2 is fixed to be 0.00481 Ωm^2). The results are shown in Fig. 10, where the true value of cell SoC is based on ampere hour counting (or $SoC_{k+1} = SoC_k + \eta_c I_k \Delta t / C_n$). It appears that all three estimators track the cell SoC reasonably well. In all cases, an initial guess of SoC closer to its true value helps the EKF converge faster. The tracking of SoC appears to be independent of the initial guess after some initial dynamics. When both R_1 and R_2 are fixed, the estimated SoC by state estimation quickly converges to the true value, however, the largest relative error is about 3% (see Fig. 11). The joint estimation of either R_1 or R_2 along with SoC provides more accurate tracking of SoC once it converges (the largest error is about 1% in Fig. 11).

When joint estimation is used, one battery parameter (either R_1 or R_2 but not both) is estimated by EKF, as shown in Fig. 12. The fixed R_1 and R_2 used in state estimation are provided as references. It appears that R_1 or R_2 in joint estimation fluctuates around the value determined by Eq. (12) shown earlier. Relaxing the fixed constraint of R_1 or R_2 allows the EKF to perform better. This is expected because the EIS indicates that the battery impedance response curve varies with respect to SoC.

In the last case study, a comparison of joint estimations of SoC and R_2 is made using different sets of model parameters shown in Table 1 in the equivalent circuit model. The initial guess of SoC is set to be 0.7 in all cases. The results are shown in Fig. 13. Despite different R_1, α and R_k used and different R_2 filtered by the EKF, all three sets of model parameters yield almost identical results of SoC after some initial dynamics.

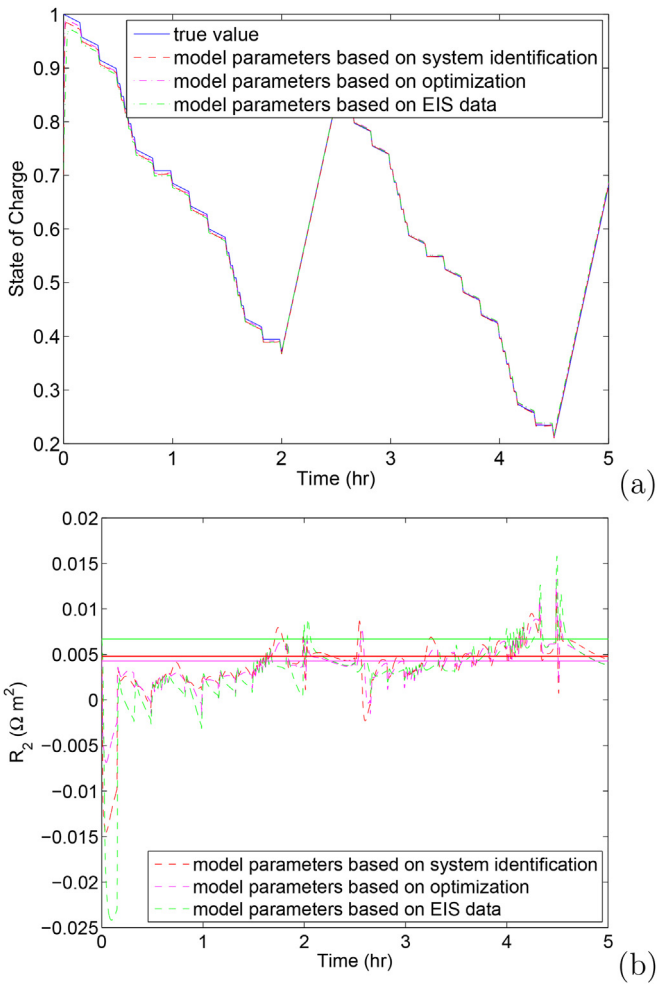

Fig. 13. Comparison of joint estimations of (a) state of charge and (b) R_2 using three sets of model parameters in the equivalent circuit model.

4. Conclusions

EIS simulations of a polymer Li-ion cell indicate that its impedance response depends on SoC. Therefore it is not possible to use an equivalent circuit model with constant parameters to describe cell dynamics at all SoCs. Relaxing the constraint of fixed R_1 or R_2 (but not both due to observability issue) in the equivalent circuit model enables the EKF algorithm to better track SoC during charge/discharge cycles.

Acknowledgements

The author would like to thank Dr. Yiming Lou (currently battery algorithm engineer at Apple Inc.), Mr. Jay Marsh (currently vice president of Innovega, Inc.), and Dr. Thomas Sobota (president of Advanced Projects Research, Inc.) for introducing him into the field of battery and for the opportunity to collaborate on design and demonstration of high-voltage, high-power Li-ion battery management systems (sponsored by U.S. Air Force) years ago.

References

[1] P.D. Christofides, Nonlinear and Robust Control of Partial Differential Equation Systems: Methods and Applications to Transport-reaction Processes, Birkhäuser, Boston, 2001.
[2] M. Cugnet, I. Baghdadi, M. Perrin, Electrochemical impedance spectroscopy of a LiFePO4/Li half-cell, in: Proceedings of the COMSOL Conference, 2012.
[3] B. Diouf, R. Pode, Potential of lithium-ion batteries in renewable energy, Renew. Energy 76 (2015) 375–380.
[4] M. Doyle, J.P. Meyers, J. Newman, Computer simulations of the impedance response of lithium rechargeable batteries, J. Electrochem. Soc. 147 (2000) 99–110.
[5] M. Doyle, J. Newman, A.S. Gozdz, C.N. Schmutz, J.M. Tarascon, Comparison of modeling predictions with experimental data from plastic lithium ion cells, J. Electrochem. Soc. 143 (1996) 1890–1903.
[6] J. Fan, Studies of 18650 cylindrical cells made with doped LiNiO2 positive electrodes for military applications, J. Power Sources 138 (2004) 288–293.
[7] L. Guo, Estimating time-varying parameters by the Kalman filter based algorithm: stability and convergence, IEEE Trans. Autom. Contr. 35 (1990) 141–147.
[8] Q.Z. Guo, R.E. White, Cubic spline regression for open-circuit potential curves of a Lithium-Ion battery, J. Electrochem. Soc. 152 (2005) A343–A350.
[9] H. He, R. Xiong, J. Fan, Evaluation of lithium-ion battery equivalent circuit models for state of charge estimation by an experimental approach, Energies 4 (2011) 582–598.
[10] B.Y. Liaw, G. Nagasubramanian, R.G. Jungst, D.H. Doughty, Modeling of lithium ion cells - a simple equivalent-circuit model approach, Solid State Ionics 175 (2004) 835–839.
[11] O.S. Mendoza-Hernandez, H. Ishikawa, Y. Nishikawa, Y. Maruyama, Y. Sone, M. Umeda, State of charge dependency of graphitized-carbon-based reactions in a lithium-ion secondary cell studied by electrochemical impedance spectroscopy, Electrochim. Acta 131 (2014) 168–173.
[12] T. Mesbahi, A. Ouari, T. Ghennam, E. Berkouk, N. Rizoug, N. Mesbahi, M. Meradji, A stand-alone wind power supply with a li-ion battery energy storage system, Renew. Sust. Energ. Rev. 40 (2014) 204–213.
[13] M. Naumann, R.C. Karl, C.N. Truong, A. Jossen, H.C. Hesse, Lithium-ion battery cost analysis in PV-household application, Energy Procedia 73 (2015) 37–47.
[14] O.M. Neamtu, M.I. Gordan, N.D. Trip, A geothermal thermo-electric energy converter for charging lithium-ion battery, in: International Symposium on Fundamentals of Electrical Engineering, IEEE, 2014, pp. 1–4.
[15] J. Newman, K.E. Thomas, H. Hafezi, D.R. Wheeler, Modeling of lithium-ion batteries, J. Power Sources 119 (2003) 838–843.
[16] I.J. Ong, J. Newman, Double-layer capacitance in a dual lithium ion insertion cell, J. Electrochem. Soc. 146 (1999) 4360–4365.
[17] S. Piller, M. Perrin, A. Jossen, Methods for state-of-charge determination and their applications, J. Power Sources 96 (2001) 113–120.
[18] G.L. Plett, Extended kalman filtering for battery management systems of LiPB-based HEV battery packs Part 2. Modeling and identification, J. Power Sources 134 (2004) 262–276.
[19] G.L. Plett, Extended kalman filtering for battery management systems of LiPB-based HEV battery packs Part 3. State and parameter estimation, J. Power Sources 134 (2004) 277–292.
[20] P. Ramadass, B. Haran, R. White, B.N. Popov, Mathematical modeling of the capacity fade of Li-ion cells, J. Power Sources 123 (2003) 230–240.

[21] K. Reif, S. Gunther, E. Yaz, R. Unbehauen, Stochastic stability of the discrete-time extended Kalman filter, IEEE Trans. Autom. Contr. 44 (1999) 714–728.
[22] J. Richardson, 50,000 battery packs to help power Israeli thermal solar plant, October 2015.
[23] S. Santhanagopalan, R.E. White, State of charge estimation using an unscented filter for high power lithium ion cells, Int. J. Energy Res. 34 (2010) 152–163.
[24] T.H. Sobota, Y. Lou, M.A. Johnson, Advanced power management technology for high-voltage high-power batteries, in: Proceedings of the 42nd Power Sources Conference, 2006.
[25] R. Spotnitz, Simulation of capacity fade in lithium-ion batteries, J. Power Sources 113 (2003) 72–80.
[26] F. Sun, X. Hu, Y. Zou, S. Li, Adaptive unscented kalman filtering for state of charge estimation of a lithium-ion battery for electric vehicles, Energy 36 (2011) 3531–3540.
[27] M. Swierczynski, D. Stroe, A. Stan, R. Teodorescu, Lifetime and economic analyses of lithium-ion batteries for balancing wind power forecast error, Int. J. Energy Res. 39 (2015) 760–770.
[28] K.M. Tsang, W.L. Chan, State of health detection for lithium ion batteries in photovoltaic system, Energ. Convers. manage. 65 (2013) 7–12.
[29] M.W. Verbrugge, R.S. Conell, Electrochemical and thermal characterization of battery modules commensurate with electric vehicle integration, J. Electrochem. Soc. 149 (2002) A45–A53.
[30] D. Zhang, B.S. Haran, A. Durairajan, R.E. White, Y. Podrazhansky, B.N. Popov, Studies on capacity fade of lithium-ion batteries, J. Power Sources 91 (2000) 122–129.

Please cite this article in press as: M. Li, Li-ion dynamics and state of charge estimation, Renewable Energy (2016), http://dx.doi.org/10.1016/j.renene.2016.06.009